Development, characterization and photocatalytic study of biocomposites based on PTFE, TiO2 and luffa cylindrica fibers

Mounir Sahli, Steve Rudz, Khaled Chetehouna, Rabah Bensaha, Mourad Korichi

Version of Record: https://www.sciencedirect.com/science/article/pii/S0254058423003437
Manuscript_8bdb4481895896959d8cd0e8a80e72cb

Development, Characterization and Photocatalytic study of biocomposites based on PTFE, TiO_2 and *luffa cylindrica* fibers

Mounir Sahli[1], Steve Rudz[2], Khaled Chetehouna[3], Rabah Bensaha[1], Mourad Korichi[4]*

**corresponding author: steve.rudz@univ-orleans.fr*

[1] Constantine Ceramics Laboratory, Université des Frères Mentouri Constantine 1, Constantine, Algeria.

[2] GREMI, UMR 7344, Université d'Orléans/CNRS, F-18020, Bourges Cedex, France

[3] INSA Centre Val de Loire, Laboratoire PRISME, EA 4229, 18020 Bourges, France

[4] Université Ouargla, Faculté des Sciences Appliquées, Laboratoire Dynamique, Interactions et Réactivité des Systèmes, BP 511 Ouargla, Algeria

Abstract: The present study focuses on the use of *Luffa Cylindrica* fibers as a reinforcing agent in a fluoroplastic (PTFE) polymer matrix and TiO_2 nanoparticles as a photocatalytic agent with different mass fractions (%), for the purpose of the preparation and structural characterization of a new biocomposite material. The granulometry and zeta potential were measured using dynamic light scattering and laser Doppler velocimetry respectively. Structural and vibrational properties of the PTFE/TiO_2/*LC* fibers composites were characterized by micro-Raman spectroscopy in oblique backscattering configuration and FTIR spectroscopy. Lastly, thermal properties were investigated using TGA and DSC. Further, the photocatalytic activity of samples was tested for the degradation of Methylene Blue dye (MB) in aqueous medium.

Keywords: *luffa cylindrica*, biocomposite, photocatalytic activity, TGA, DSC.

1. Introduction

Biopolymer composites offer promising properties in terms of biocompatibility, biodegradability, abundant availability, specific rigidity, flexibility over processing, and control of the overall polymer permeability[1–5]. These properties are classified into two groups: environmental and mechanical. The development of these materials is due to environmental concerns: while synthetic polymers derived from petroleum are widely used and exhibit satisfying mechanical properties, their environmental cost is no longer acceptable. Following the advent of environmental awareness a few decades ago, biocomposites have since then been successfully used in many areas of human activity as substitutes for synthetic ones: the automotive industry[6,7], construction materials in civil engineering[8,9], aerospace engineering[10,11], packaging[12,13], maritime industries[14,15], textiles[16,17], agriculture[18,19], electronics[20,21], medicine and pharmaceutical industries[22–25], and some others[26,27].

Many natural species have already been investigated to find suitable ones for these applications. Several studies have pointed out the mechanical and acoustic properties of *Luffa Cylindrica*[28–30], and also reported its potential in the textile industry and in environmental and bioprocess engineering where it can be used to remove chromium III, cadmium and nickel II ions from contaminated aqueous media[31,32]. It also has interesting medical properties as some of its chemical components (phenolics, lavonoids, oleanolic acid, ascorbic acid, a-tocopherol, carotenoids, chlorophylls, triterpenoids and ribosome-inactivating proteins) are of great value as anti-inflammatory agents or as immunostimulants for example[33].

Luffa Cylindrica (*LC*) is an annual species of vine classified in the cucurbitaceous family[34]. This plant is common in tropical and sub-tropical regions from North Africa to South and Southeast Asia and in South America[35]. It produces a fruit with a cylindrical shape and an internal structure similar to a sponge with a cellulose fibril arrangement forming a fibrous vascular system[36]. The fibers are mainly made of cellulose (63.0 ± 2.5)%, lignin (11.7 ± 1.2)%, hemicelluloses (20.9 ± 1.4)% and ash (0.4 ± 0.1)%[35–38] and are shaped as continuous hollow microchannels with a diameter of 10-20 μm up to 800 μm for the macropores[39–41].

The choice of the matrix to use with *LC* depends on its application. For example, the use of a polyurethane matrix is suitable for building materials where thermal stability and acoustic properties are important criteria[35]. In the present study, the matrix was made of titanium dioxide-polytetrafluorethylene (TiO_2-PTFE). Its antibacterial and anti-corrosion properties are of great interest in medical science for implant purposes where implant-related infections and complications are problematic[42,43].

The aim of the present work was to develop and characterize a new biocomposite material based on *Luffa Cylindrica* fibers as reinforcing agents in a fluoroplastic polytetrafluoroethylene (PTFE) polymer matrix and TiO_2 nanoparticles as photocatalytic agents at various mass fractions (%).

2. Experimental methodology

2.1. Sample characteristics and preparation

The three materials used in this study are shown in Figure 1. The first material, nanoparticles of titanium dioxide (Degussa P25 TiO_2), is commonly used in photocatalytic reaction systems due to its high level of activity. The particles have a spherical shape and a specific surface area of 51 m^2. Its anatase/rutile composition is 70:30. The second material used is polytetrafluorethylene (PTFE) as the main element of the matrix alongside the titanium dioxide. This material is well-known for its low friction and non-reactivity qualities, finding applications from wiring in aerospace to nonstick pans in the kitchen. The third material is the fibers of *Luffa Cylindrica*. The fibers, used as a reinforcement agent in the PTFE matrix, were collected from the Mediterranean region. This material is not manufactured like the other two and its preparation is presented here. Dry fruits of *Luffa Cylindrica* were collectedin the north-east of Algeria in a region named Constantine. The harvested fruits were washed several times with distilled water, then dried at ambient temperature during three days and finally dried about thirty minutes at 110 °C. Once this step had been completed, the fibers were cut into small pieces and then ground at a temperature of about -196 °C *via* a cryogenic grinding process. This process yields similar particle sizes in terms of granulometry and also maintains the initial chemical and physical properties of the fibers. The powder thus obtained was then sieved for 20 minutes in order to select only particles with a size below 200 μm. The selected fibers were finally washed and dried a last time to eliminate any residual contaminants. The whole procedure of the *LC* fibers preparation is summed up in Figure 2. The obtained fibers were visualized using light microscopy (Euromex, Holland) equipped with a digital camera system (CMEX 5000). The fibers morphology analysis was performed by Image Focus software. The *Luffa cylindrica* fibers shown in Figure 1(d) are heterogeneously distributed with different shapes; their length can reach several tens of micrometers.

Once all the materials had been individually prepared, the PTFE/TiO_2/*LC* fibers biocomposite samples were prepared by manual milling. An analytical balance was used to weigh the three basic compounds, which were then sieved and mixed together by vigorous manual milling in a mortar for approximately 15 minutes.

Three different mass fractions were considered for the samples, as reported in Table 1, in order to produce a biocomposite material at the percolation threshold.

Finally, the samples are formed into cylindrical pellets with 13 mm in diameter and 4.4 mm in thickness using a hydraulic press to compress the sample into powder form in a pelletizer (the force applied is 5 metric tons), see Fgure 3(a). Figure 3(b) shows the scanning electron microscopy images (SEM) and Elemental analysis (EDAX) of sample 2, obtained using a ZEISS GeminiSEM 500 with a field emission Schottky source equipped with an EDAX SDD for chemical analysis. For the surface composition of the samples, we notice the presence of chlorine due to the use of commercial TiO_2, which was synthesized by the chloride process according to the following reaction: $TiCl_4 + O_2 \rightarrow TiO_2 + 2Cl_2$

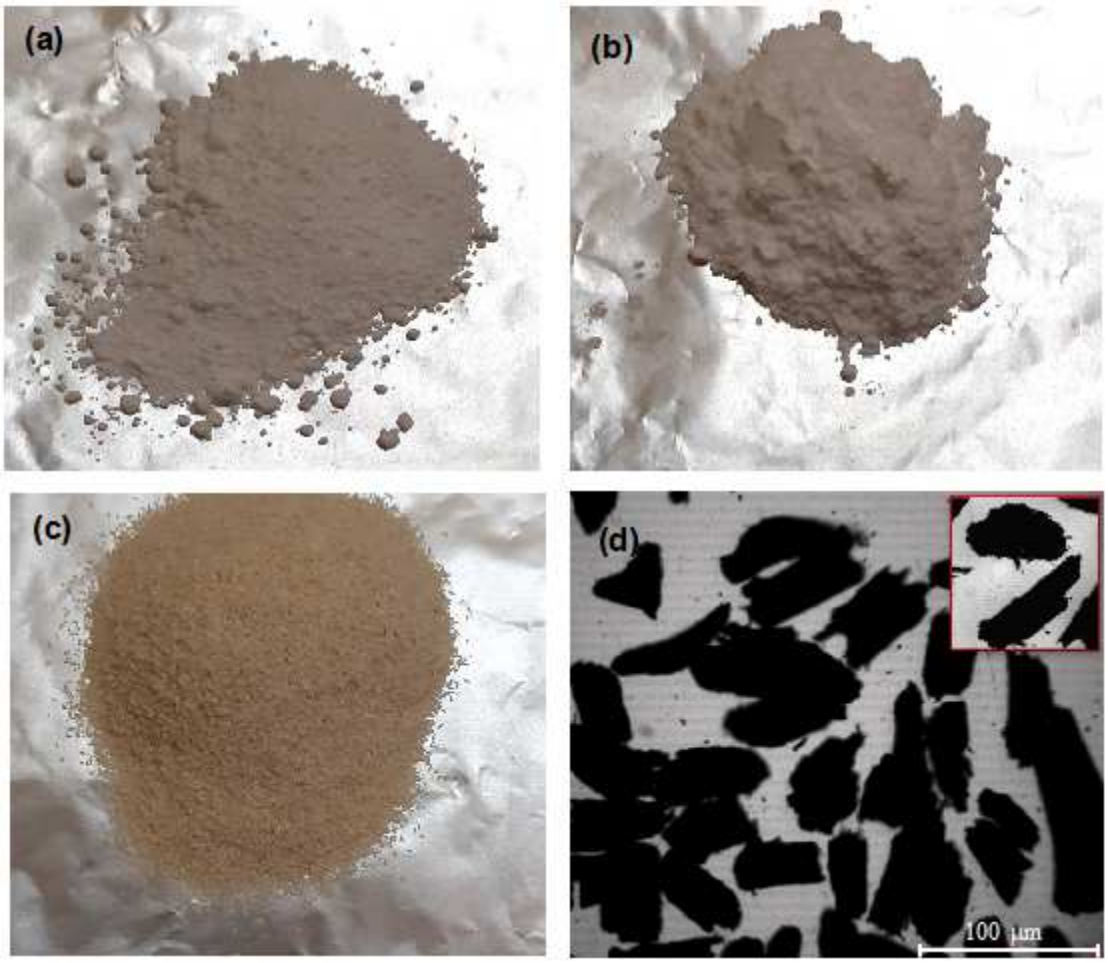

Figure 1. Ground materials used in the present study. **(a)** Degussa P25 TiO_2. **(b)** Polytetrafluorethylene (PTFE). **(c)** *Luffa Cylindrica* fibers. **(d)** microscopic photo showing the spatial distribution, shapes, and sizes of the obtained fibers.

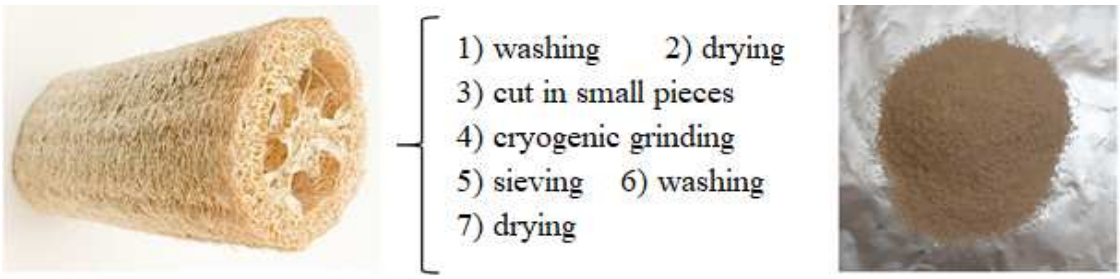

Dry collected fruit Preparation steps *LC* fibers obtained

Figure 2. Preparation steps of *Luffa Cylindrica* fibers

Table 1. Mass fractions of the studied samples

Sample number	**PTFE (%)**	**TiO_2 (%)**	***LC* fibers (%)**
1	65	5	30
2	70	5	25
3	60	5	35

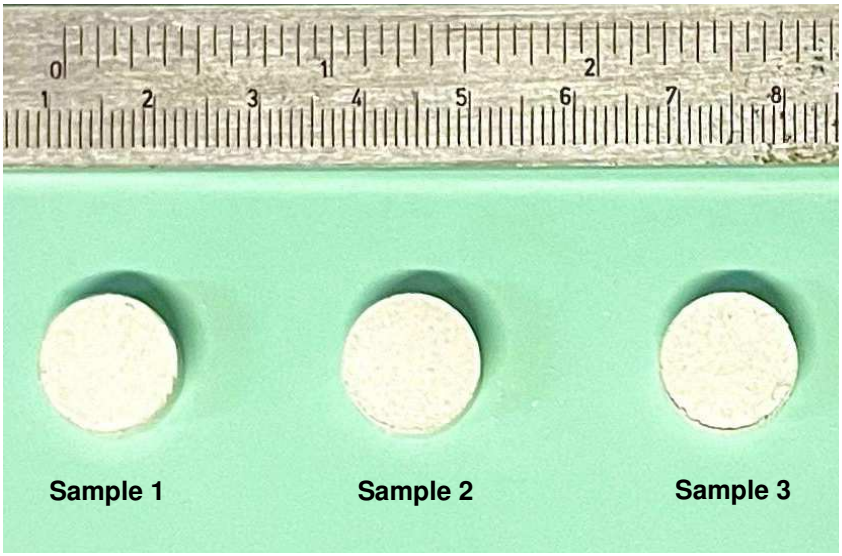

(a)

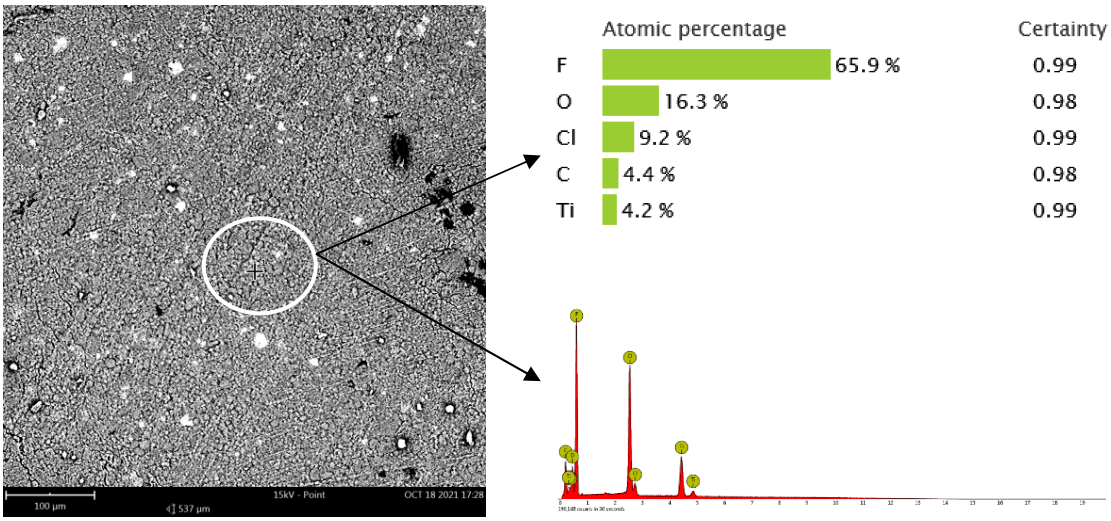

(b)

Figure 3. (a) Example of samples, (b) Scanning electron microscopy images (SEM) and Elemental analysis (EDAX) of sample 2.

2.2. Characterization

The samples were characterized using the following methods: general properties with particle size and zeta potential measurements, structural and vibrational properties with spectroscopic approaches (both Raman and Infrared) and thermal properties by both thermogravimetric and differential scanning calorimetry analysis.

The particle size of the studied biocomposite was investigated by dynamic light scattering (ZetasizervNano ZS90; Malvern Instrument Ltd., GB). All the samples were reduced to powder and then diluted in distilled water with a concentration up to 1 mg/mL and a pH of 6 prior to its injection in the analyzer device. The light used in this apparatus was a He-Ne laser source (wavelength of 633 nm) and the scattering angle was 90°. During all experiments, the gain and shutter settings remained constant. The same apparatus was used to determine the zeta potential, but instead of light scattering the technique employed was laser doppler microelectrophoresis. This technique measures the electrophoretic mobility from which the zeta potential is then deduced *via* the Smoluchowski equation, Equation (1):

$$\boldsymbol{\mu_{ep}} = \frac{\boldsymbol{\varepsilon_0 \varepsilon_r}}{\boldsymbol{\eta}} \boldsymbol{\zeta} \qquad (1)$$

with $\boldsymbol{\mu_{ep}}$ the electrophoretic mobility of a particle in $m^2.V^{-1}.s^{-1}$, $\boldsymbol{\varepsilon_0}$ the vacuum permittivity in $C.V^{-1}.m^{-1}$, $\boldsymbol{\varepsilon_r}$ the dielectric constant of the medium, $\boldsymbol{\eta}$ the viscosity of the medium in Pa.s and $\boldsymbol{\zeta}$ the zeta potential in V.

The structure of the biocomposite was then investigated with two spectroscopic approaches, Raman spectroscopy and FTIR. Raman spectroscopy was used to characterize the molecular structure of the samples. Raman spectra were recorded with a micro-Raman spectrometer in backscattering mode (SENTERRA R200-L with a CCD sensor cooled at -65°C). The excitation wavelength was 785 nm and obtained with an Ar laser and the laser power was fixed at 100 mW during the experiments. In all experiments, the exposure time was 10 s and spectra were recorded in continuous scanning mode from 400 to 4000 cm^{-1}. The second, complementary spectroscopy approach, Fourier Transform InfraRed spectroscopy (FTIR), was performed on the samples with a Jasco FT/IR-6300 type A (Jasco Analytical Instruments, Easton, MD, USA) coupled with an Attenuated Total

Reflection module (ATR PRO450-S, 45° incident angle). All spectra were collected with a resolution of 4 cm^{-1} in continuous scanning mode (speed rate of 2 $mm.s^{-1}$) from 4000 to 500 cm^{-1}.

The thermal properties of the samples were studied using thermogravimetric analysis (TGA) and Differential Scanning Calorimetry (DSC) with the ATR method and a TGS detector. These analyses were performed simultaneously for all samples. The device used was a Jupiter STA 449 F3 calorimeter by NETZSCH (NETZSCH, Selb, Germany) with an Al_2O_3 crucible. On all tests, the scanning speed was 2 $mm.s^{-1}$, the temperature range 24-320 °C with a heating rate of 10 $°C.min^{-1}$, and all experiments were performed in Argon atmosphere with a flow rate of 20 $mL.min^{-1}$.

2.3 Photocatalytic testing

The photocatalytic activity of the three samples was estimated by measuring the rate constant and the degradation rate of MB in aqueous solution under UV light irradiation. The experiment was carried out in a 100 mL beaker with artificial light emitting at 365 nm. Before starting the photocatalytic tests, a mass of (0.8 ± 0.1) g of the catalyst in the tablet form with a diameter of 1.3 cm and a thickness of 0.2 cm was added to 50 mL of methylene blue solution with an initial concentration of 10 ppm at free pH. To establish adsorption equilibrium, the mixture was constantly magnetically stirred in the dark for 30 minutes. Absorbance measurements were made at equal time intervals using a JASCO V-630 UV/Visible spectrophotometer.

The experimental values of the rate constant $\boldsymbol{K}$ (min^{-1}) and the degradation rate $\boldsymbol{D\%}$ are obtained using the following equations (2) and (3):

$$\boldsymbol{ln\left(\frac{C_0}{C}\right) = K.t} \qquad (2)$$

$$\boldsymbol{D\% = 100.\left(1 - \frac{C}{C_0}\right)} \qquad (3)$$

Where $\boldsymbol{C_0}$ is the initial concentration of MB (ppm), $\boldsymbol{C}$ is the residual concentration (ppm), and t is the irradiation time (min).

3. Results and discussion

The first experiment carried out was granulometry to check any anomalies. The measured granulometry of the 3 samples presented in Figure 4 revealed the absence of anomalies, with peak values of 91.28, 105.7 and 91.28 nm and polydispersity indexes of 16.6, 16.8 and 15.8% for samples 1, 2 and 3 respectively.

Table 2 presents the zeta potential of the three samples with their associated electrophoretic mobility and conductivity. The experiments were reproducible, with a standard deviation for the electrophoretic mobility measurements below 0.5 $\mu m.cm.V^{-1}.s^{-1}$. The results show that the zeta potential for the three samples was in the same range; the highest absolute value was found for sample 2. Their associated zeta potential distributions are given in Figure 5. The conductivity was the same order of magnitude for all the samples. In terms of electrostatic

stabilization, sample 2 with the lowest mass fraction of *LC* (70%PTFE/5%TiO_2/25%*LC*) yielded the best performance with the highest zeta potential (in absolute value), indicating a rise in interparticle forces. The reported value for sample 2, very close to 30 mV in absolute value, is indicative of a reasonably stable dispersion. It is also interesting to point out that the zeta potential of sample 3 (with the highest mass fraction of *LC*) is lower than that of sample 1 (*LC* mass fraction between sample 1 and 2).

Table 2. Zeta potential, mobility and conductivity of the three samples.

Sample	Zeta potential (mV)	Mobility (µm cm/Vs)	Conductivity (mS/cm)
Sample 1	-25.8	-1.781	0.0961
Sample 2	-29.2	-2.017	0.0346
Sample 3	-27.5	-1.899	0.0271

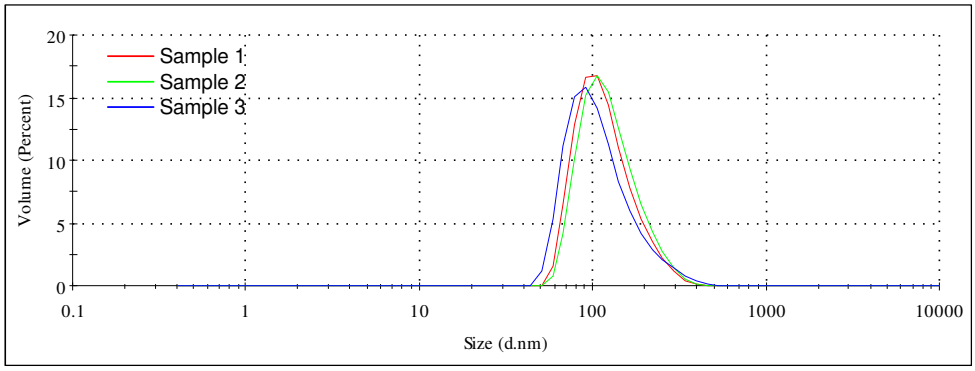

Figure 4. Particle size distribution of the three samples.

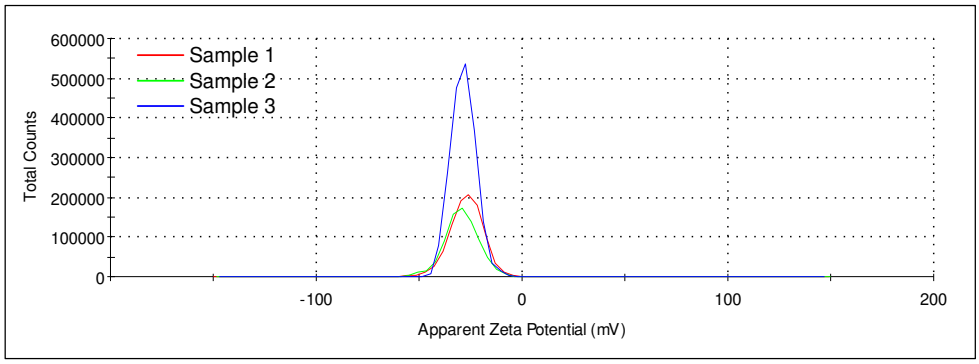

Figure 5. Apparent zeta potential distribution of the three samples.

Then, the structural and vibrational properties were assessed using Raman spectroscopy and FTIR spectroscopy. Figure 6 presents the Raman spectra obtained for all samples. All the curves were shape-similar, only the peak amplitudes varied slightly from one sample to another. Consequently, the structural characteristics of all the samples are the same. Raman peaks at 144 cm^{-1} (E_g mode), 198.5 cm^{-1} (E_g mode), 392.5 cm^{-1} (B_{1g} mode), 517.5 cm^{-1} (A_{1g} + B_{1g} mode) and 638 cm^{-1} (E_g mode) were recorded for the three sample configurations and were assigned to the Raman active modes of the anatase crystal[44,45]. The peak located at 445.5 cm^{-1} is characteristic of rutile in TiO_2 (Eg mode)[45,46]. The last two Raman peaks recorded at 1200 cm^{-1} and 1293 cm^{-1} are $\nu_{asym}(CF_2)$ and ν (C–C) stretching vibrations respectively[47]. The FTIR-spectra of the three samples are presented in Figure 7a and b and Table 3 summarizes all the IR absorption peaks and their interpretations. As in

the Raman experiments, the three spectra are almost identical. Concerning the lowest frequencies (400 to 800 cm^{-1}, Figure 7b), where vibration is from organometallic molecules, the three recorded peaks come from the stretching vibration mode of Ti-O[48]. The observed middle frequencies (800 to 1500 cm^{-1}, Figure 7b) are due to cellulose[49]. The highest observed frequencies (2908.13, 2982.37 and 3661.19 cm^{-1}, Figure 7a) are caused by the vibration modes of water and organic molecules.

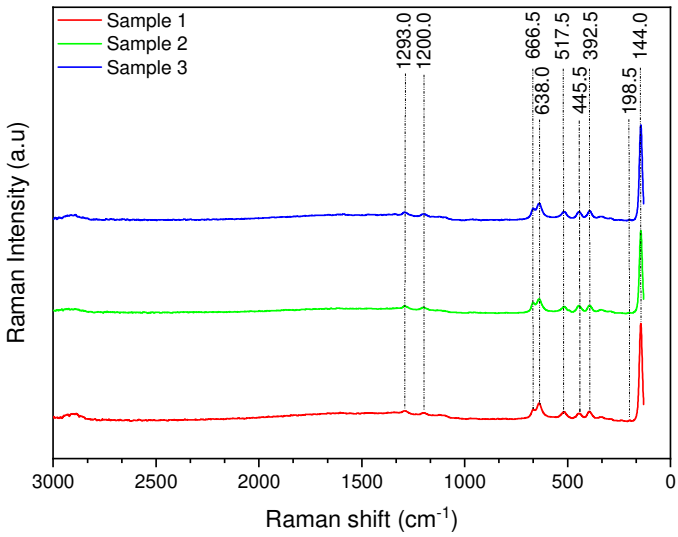

Figure 6. Raman spectra for the three samples.

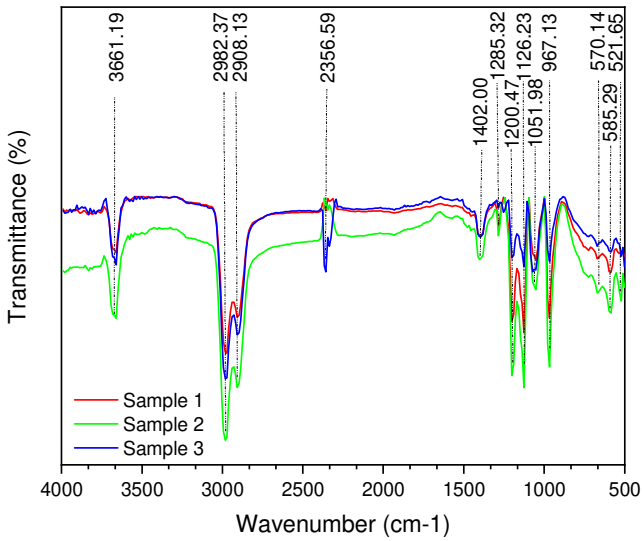

Figure 7a. Whole FTIR spectra for the three samples.

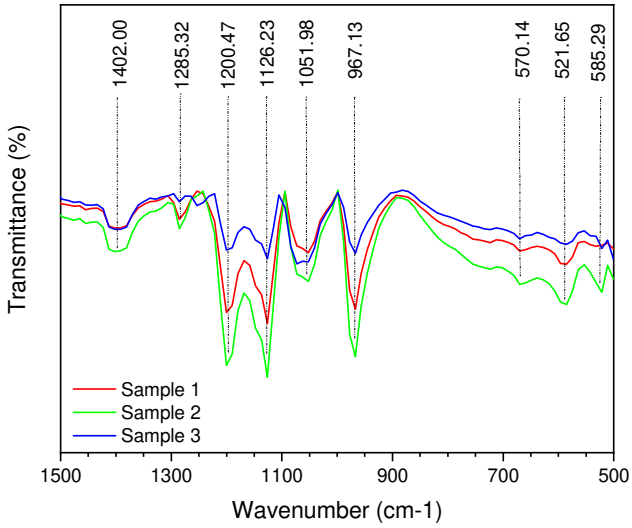

Figure 7b. FTIR spectra for the three samples for the lowest wavenumber.

Table 3. FTIR transmittance peaks and their assignments.

Wavenumber (cm^{-1})	**Assignments**
3661.19	OH stretching of cellulose and hemicellulose.[50,51]
2982.37	CH stretching of cellulose and hemicellulose.[50,51]
2908.13	Asymmetric CH_2 stretching in long alkyl chain.[50,51]
2360.00	Symmetric stretching of the carboxyl C=O band.
1402.00	Characteristic of carboxylic vibration in pectins.
1285.32	CF stretching.[51,52]
1200.47	OH in-plane bending CF_2 stretching.[52–54]
1126.23	CF_3 symmetric stretching.[53]
1051.98	Asymmetric in-plane ring stretch.[50,51]
967.13	CH out-of-plane deformation of double bonds with trans configuration.[55].
670.14	CF_2 wagging.[51,52]
585.29	CF_2 wagging.[51,52]
521.65	Ti–O–Ti stretching vibration.[56]

Lastly, thermal degradation was investigated using TGA and DSC. The results of the analyses are presented on Figures 8 and 9 for DSC and TGA respectively. Both the 3 samples and the *LC* fibers alone were tested. The DSC results on the 3 samples (Figure 8) show that their behaviour is very similar to that of PTFE[51], the main component in terms of mass fraction in all the samples. Moreover, it is noticeable that the glass-transition temperature about 195°C in all the biocomposite samples is the same as that of PTFE. For temperatures up to 170 °C the curves of the studied biocomposites are almost identical, but then sample 3, which has the highest mass fraction of *LC* fibers, starts to increase faster than the other two and at the same rate as the *LC* fiber sample. Above 250 °C the 3 samples exhibit the same trend again. From these observations, it is clear that the similarity of the curves for the 3 different mass fractions proposed in this work reflects the same thermal

behaviour. Consequently, for all the biocomposite samples tested a similar mechanism is involved. The TGA curve for *LC* fibers (Figure 9) is consistent with other work in the literature[38,57]: the mass loss up to a temperature of 100 °C is due to water loss, then the slight mass loss in the range 200-260 °C is due to the degradation of hemicellulose (20.9% of its initial mass) while the huge mass loss above 240 °C is the result of the degradation of cellulose (63.0% of its initial mass) starting at 240°C and the degradation of lignin (11.7% of its initial mass) starting at 280 °C. The TGA curves for the 3 different biocomposites show the same trend in that the thermal degradation related to its kinetic is temperature dependent. Together with the DSC analysis, one can again assume that there is a unique governing mechanism. On these 3 biocomposite curves, two significant temperature ranges can be identified. From 30 to 230 °C, the mass remains quasi-constant, which implies weak thermal agitation and consequently negligible diffusion. Above 230 °C the mass loss becomes significant. As PTFE is not subject to mass loss in these types of tests[51], and as the TiO_2 mass fraction is not large enough (5%) to have a significant impact on mass loss, the reported mass loss is attributed to degradation of the *LC* fibers. To give a figure, at the highest temperature (350°C) the reported mass ratios are 81%, 85% and 77% for sample 1, 2 and 3 respectively and 40% for *LC* fibers. Considering only *LC* fibers mass loss yields mass ratios of 82%, 85% and 79% at a temperature of 350 °C and supports the assumption of *LC* fibers degradation as the main cause of mass loss.

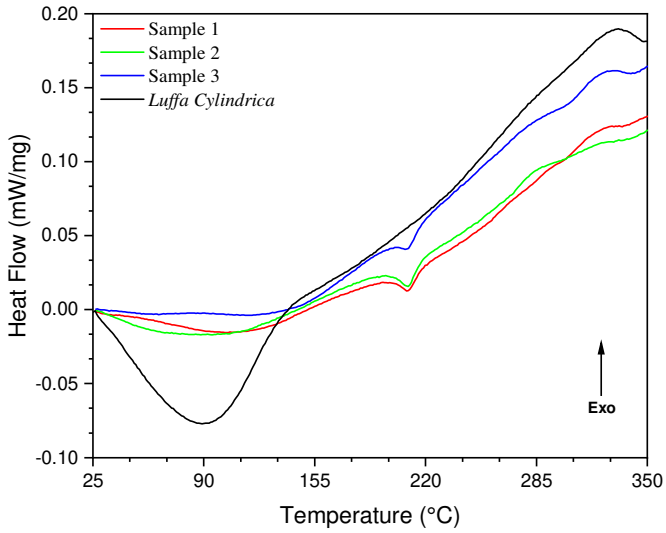

Figure 8. DSC-curves for the three samples and *LC* fibers.

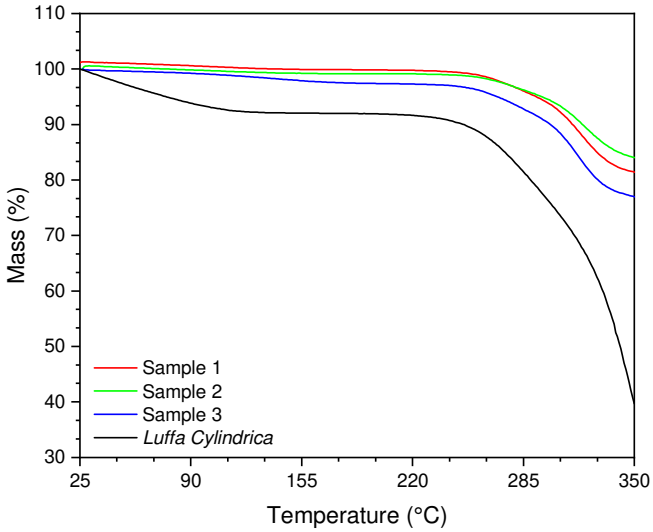

Figure 9. TGA-curves for the three samples and *LC* fibers.

The prepared samples were tested on photodegradation of Methylene Blue dye in this study. The latter in aqueous solution absorbs in the visible light (λmax = 651 nm). To verify the Beer-Lambert law (equation (2)) and the degradation rate (equation (3)), absorbance measurements of several MB solutions at known concentrations were performed. Figure 10 shows the results obtained. It can be seen that this curve is linear over the range of concentrations selected with a regression coefficient R^2= 0.99, showing that the Beer-Lambert law is verified over this concentration range.

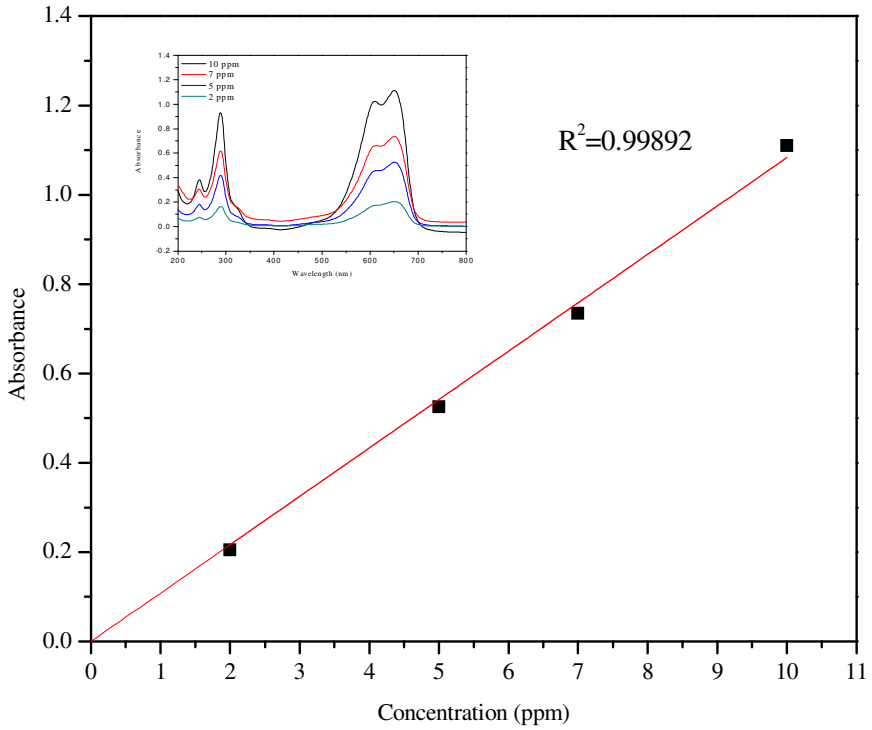

Figure 10. The Spectrophotometer calibration curve of Methylene Blue dye at λ = 651 nm.

Figure 11(a) shows the measured variation of C/C_0 as a function of time for the three samples. From this data, the logarithm of the C/C_0 in function of time is computed in Figure 11(b) and it can be seen that all curves are linear over the range of concentrations selected with a regression coefficient R^2 greater than 0.99 for all curves. Accordingly, the apparent rate K (min^{-1}) is then deduced and presented in Table 4. The photocatalytic efficiency of sample 3 is higher due to the increase in *LC* fibers (35%). This increased surface area also increases the number of active sites. About the degradation rate *D%*, in Figure 12(a), we observed a progressive discoloration of the solution and a rapid disappearance of 94.7% after 210 minutes of irradiation in the presence of the sample 3 while it is only 53.96 for the sample 2 and 81.4% for the sample 1. This result highlights that the dye degradation kinetic is an increasing function of *LC* fibers' mass fraction. The rate of disappearance of this dye follows the Langmuir-Hinshelwood (L-H) model. However, photocatalysis by biomaterials based on natural fibers is a rapid and effective method for the degradation of organic pollutants, in particular methylene blue.

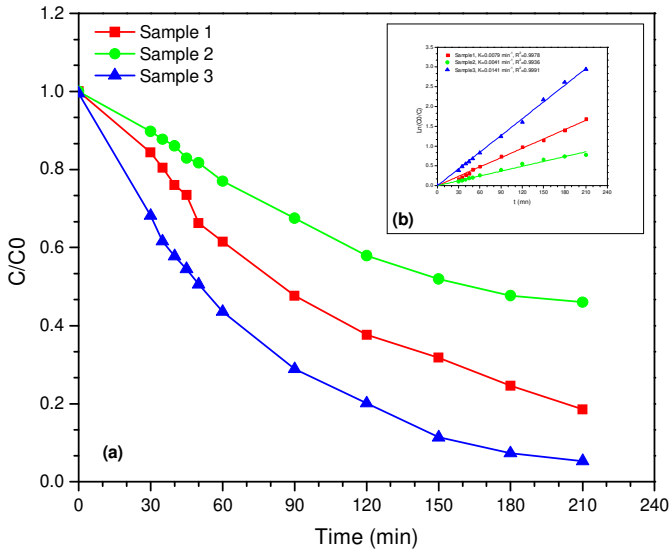

Figure 11. (a) The temporal variation of C/Co for the three samples, (b) The temporal variation of ln (Co/C) for the three samples.

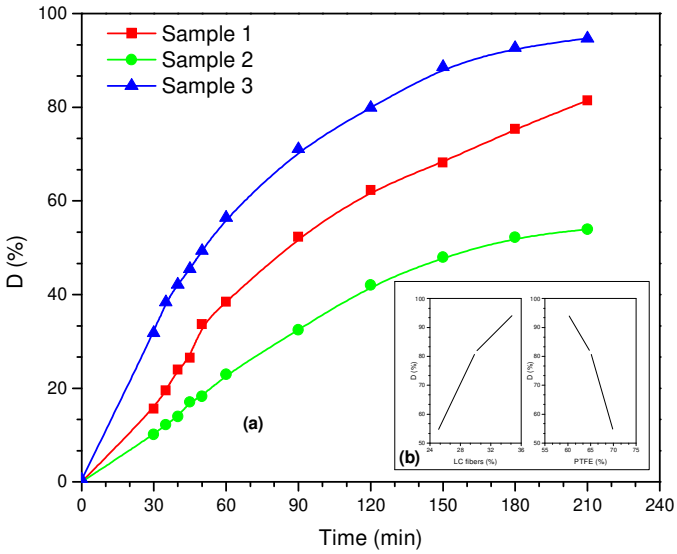

Figure 12. (a) The temporal variation of degradation rate for the three samples, **(b)** Variation of the degradation rate as a function of *LC* and PTFE mass fractions.

Table 4. Degradation rate D% and apparent rate constant values K of the samples.

Sample	K(min^{-1})	Standard Error (min^{-1})	Adj. R-Square R^2	D (%)
1	0.00787	$1.05977E^{-4}$	0.9978	81.4
2	0.00407	$9.43658E^{-5}$	0.9936	54.0
3	0.01409	$1.22064E^{-4}$	0.9991	94.7

4. Conclusion

This work experimentally characterized the structural properties of a new biocomposite based on polytetrafluorethylene (PTFE), titanium dioxide (TiO_2) and fibers of *Luffa Cylindrica* (*LC*). In this biocomposite TiO_2 (P25) was used, with the same mass fraction in all tested samples, for its photocatalytic ability, and *LC* as a reinforcement agent. The three sample configurations were (in terms of mass fraction) {PTFE: TiO_2: *LC*} = {(65: 5: 30); (70: 5: 25); (60: 5: 35)}%. The granulometry yielded peaks centered at 91.28, 105.7 and 91.28 nm with similar associated polydispersity indexes of 16.6%, 16.8% and 15.8% for samples 1, 2 and 3 respectively. Their zeta potentials were -25.8, -29.2 and -27.5 mV for configuration 1, 2 and 3 respectively. Consequently, configuration 2 (70: 5: 25) % outperformed the others in terms of electrostatic stabilization. In all samples, FTIR spectra and Raman spectra highlighted the presence of specific bands of cellulose, hemicellulose and PTFE. Moreover, Raman spectra showed vibrational bands attributed to the presence of anatase and rutile phases of TiO_2, with corresponding peaks of ν_{asym} (CF_2) and ν (C–C). Lastly, the thermal degradation properties are similar for samples 1 and 2, and outperform those of sample 3. Methylene Blue dye degradation was used to study the photocatalytic activity. A higher photocatalytic efficiency of 94.7% was obtained with sample 3 (35% *LC* fibers, 5% TiO_2 and 60% PTFE), due to the large surface area and thus the number of active sites.

The next step in this work will be the characterization of this new biocomposite in terms of its mechanical and tribological properties. The numerical investigation of the heat transfer in this material under fire stress will also be investigated [58].

References

[1] P. Bordes, E. Pollet, L. Avérous, Nano-biocomposites: Biodegradable polyester/nanoclay systems, Prog. Polym. Sci. 34 (2009) 125–155. https://doi.org/10.1016/j.progpolymsci.2008.10.002.

[2] M.G. Lomelí Ramírez, K.G. Satyanarayana, S. Iwakiri, G.B. De Muniz, V. Tanobe, T.S. Flores-Sahagun, Study of the properties of biocomposites. Part I. Cassava starch-green coir fibers from Brazil, Carbohydr. Polym. 86 (2011) 1712–1722. https://doi.org/10.1016/j.carbpol.2011.07.002.

[3] P. Cataldi, M. Cassinelli, J.A. Heredia-Guerrero, S. Guzman-Puyol, S. Naderizadeh, A. Athanassiou, M. Caironi, Green Biocomposites for Thermoelectric Wearable Applications, Adv. Funct. Mater. 30 (2020) 1–10. https://doi.org/10.1002/adfm.201907301.

[4] J.R. Robledo-Ortíz, M.E. González-López, D. Rodrigue, J.F. Gutiérrez-Ruiz, F. Prezas-Lara, A.A. Pérez-Fonseca, Improving the Compatibility and Mechanical Properties of Natural Fibers/Green Polyethylene Biocomposites Produced by Rotational Molding, J. Polym. Environ. 28 (2020) 1040–1049. https://doi.org/10.1007/s10924-020-01667-1.

[5] K. Prasad, M. Nikzad, I. Sbarski, Modeling Permeability in Multi-Phase Polymer Composites: A Critical Review of Semi-Empirical Approaches, Polym. Rev. 61 (2021) 194–237.

https://doi.org/10.1080/15583724.2020.1743306.

[6] O. Akampumuza, P.M. Wambua, A. Ahmed, W. Li, X.H. Qin, Review of the applications of biocomposites in the automotive industry, Polym. Compos. 38 (2017) 2553–2569. https://doi.org/10.1002/pc.23847.

[7] T. Gurunathan, S. Mohanty, S.K. Nayak, A review of the recent developments in biocomposites based on natural fibres and their application perspectives, Compos. Part A Appl. Sci. Manuf. 77 (2015) 1–25. https://doi.org/10.1016/j.compositesa.2015.06.007.

[8] U. Riedel, J. Nickel, Natural fibre-reinforced biopolymers as construction materials - New discoveries, Angew. Makromol. Chemie. 272 (1999) 34–40. https://doi.org/10.1002/(sici)1522-9505(19991201)272:1<34::aid-apmc34>3.3.co;2-8.

[9] M.P. Ansell, M. Lawrence, Y. Jiang, A. Shea, A. Hussain, J. Calabria-Holley, P. Walker, Natural plant-based aggregates and bio-composite panels with low thermal conductivity and high hygrothermal efficiency for applications in construction, in: K.A. Harries, B. Sharma (Eds.), Nonconv. Vernac. Constr. Mater. Characterisation, Prop. Appl., Woodhead P, Elsevier Ltd, 2019: pp. 217–245. https://doi.org/10.1016/B978-0-08-102704-2.00010-X.

[10] M. Toozandehjani, Conventional and Advanced Composites in Aerospace Industry: Technologies Revisited, Am. J. Aerosp. Eng. 5 (2018) 9. https://doi.org/10.11648/j.ajae.20180501.12.

[11] P. Balakrishnan, M.J. John, L. Pothen, M.S. Sreekala, S. Thomas, Natural fibre and polymer matrix composites and their applications in aerospace engineering, in: S. Rana, R. Fangueiro (Eds.), Adv. Compos. Mater. Aerosp. Eng., Woodhead P, Elsevier Ltd, 2016: pp. 365–383. https://doi.org/10.1016/b978-0-08-100037-3.00012-2.

[12] K.K. Gaikwad, J.Y. Lee, Y.S. Lee, Development of polyvinyl alcohol and apple pomace bio-composite film with antioxidant properties for active food packaging application, J. Food Sci. Technol. 53 (2016) 1608–1619. https://doi.org/10.1007/s13197-015-2104-9.

[13] E.L. Sánchez-Safont, A. Aldureid, J.M. Lagarón, J. Gámez-Pérez, L. Cabedo, Biocomposites of different lignocellulosic wastes for sustainable food packaging applications, Compos. Part B Eng. 145 (2018) 215–225. https://doi.org/10.1016/j.compositesb.2018.03.037.

[14] M.P. Ansell, Natural fibre composites in a marine environment, in: A. Hodzic, R. Shanks (Eds.), Nat. Fibre Compos. Mater. Process. Appl., Woodhead Publishing Limited, 2014: pp. 365–374. https://doi.org/10.1533/9780857099228.3.365.

[15] K. Lau, P. Hung, M.-H. Zhu, D. Hui, Properties of natural fibre composites for structural engineering applications, Compos. Part B Eng. 136 (2018) 222–233. https://doi.org/10.1016/j.compositesb.2017.10.038.

[16] D.U. Shah, D. Porter, F. Vollrath, Opportunities for silk textiles in reinforced biocomposites: Studying through-thickness compaction behaviour, Compos. Part A Appl. Sci. Manuf. 62 (2014) 1–10. https://doi.org/10.1016/j.compositesa.2014.03.008.

[17] M.J. John, S. Thomas, Biofibres and biocomposites, Carbohydr. Polym. 71 (2008) 343–364. https://doi.org/10.1016/j.carbpol.2007.05.040.

[18] S. Iannace, G. Nocilla, L. Nicolais, Biocomposites based on sea algae fibers and biodegradable thermoplastic matrices, J. Appl. Polym. Sci. 73 (1999) 583–592. https://doi.org/10.1002/(SICI)1097-4628(19990725)73:4<583::AID-APP14>3.0.CO;2-H.

[19] G. Faludi, G. Dora, K. Renner, J. Móczó, B. Pukánszky, Biocomposite from polylactic acid and lignocellulosic fibers: Structure-property correlations, Carbohydr. Polym. 92 (2013) 1767–1775. https://doi.org/10.1016/j.carbpol.2012.11.006.

[20] P. Cataldi, F. Bonaccorso, A. Esau del Rio Castillo, V. Pellegrini, Z. Jiang, L. Liu, N. Boccardo, M. Canepa, R. Cingolani, A. Athanassiou, I.S. Bayer, Cellulosic Graphene Biocomposites for Versatile High-Performance Flexible Electronic Applications, Adv. Electron. Mater. 2 (2016). https://doi.org/10.1002/aelm.201600245.

[21] R.K. Pal, A.A. Farghaly, C. Wang, M.M. Collinson, S.C. Kundu, V.K. Yadavalli, Conducting polymer-silk biocomposites for flexible and biodegradable electrochemical sensors, Biosens. Bioelectron. 81 (2016) 294–302. https://doi.org/10.1016/j.bios.2016.03.010.

[22] H. Xie, T. Cao, F.J. Rodríguez-Lozano, E.K. Luong-Van, V. Rosa, Graphene for the development of the next-generation of biocomposites for dental and medical applications, Dent. Mater. 33 (2017) 765–774. https://doi.org/10.1016/j.dental.2017.04.008.

[23] G. Furtos, M.A. Naghiu, H. Declercq, M. Gorea, C. Prejmerean, O. Pana, M. Tomoaia-Cotisel, Nano forsterite biocomposites for medical applications: Mechanical properties and bioactivity, J. Biomed. Mater. Res. - Part B Appl. Biomater. 104 (2016) 1290–1301. https://doi.org/10.1002/jbm.b.33396.

[24] A. Abdulkhani, E. Hojati Marvast, A. Ashori, Y. Hamzeh, A.N. Karimi, Preparation of cellulose/polyvinyl alcohol biocomposite films using 1-n-butyl-3-methylimidazolium chloride, Int. J. Biol. Macromol. 62 (2013) 379–386. https://doi.org/10.1016/j.ijbiomac.2013.08.050.

[25] V. Sedlařík, N. Saha, I. Kuřitka, P. Sáha, Characterization of Polymeric Biocomposite Based on Poly(vinyl alcohol) and Poly(vinyl pyrrolidone), Polym. Compos. 27 (2006) 147–152. https://doi.org/10.1002/pc.

[26] D. Trache, M.H. Hussin, C.T. Hui Chuin, S. Sabar, M.R.N. Fazita, O.F.A. Taiwo, T.M. Hassan, M.K.M. Haafiz, Microcrystalline cellulose: Isolation, characterization and bio-composites application—A review, Int. J. Biol. Macromol. 93 (2016) 789–804. https://doi.org/10.1016/j.ijbiomac.2016.09.056.

[27] H.P.S. Abdul Khalil, C.K. Saurabh, A.S. Adnan, M.R. Nurul Fazita, M.I. Syakir, Y. Davoudpour, M. Rafatullah, C.K. Abdullah, M.K.M. Haafiz, R. Dungani, A review on chitosan-cellulose blends and nanocellulose reinforced chitosan biocomposites: Properties and their applications, Carbohydr. Polym. 150 (2016) 216–226. https://doi.org/10.1016/j.carbpol.2016.05.028.

[28] E. Jayamani, S. Hamdan, M.R. Rahman, S.K. Heng, M. Khusairy Bin Bakri, Processing and Characterization of Epoxy/Luffa Composites: Investigation on Chemical Treatment of Fibers on Mechanical and Acoustical Properties, BioResources. 9 (2014) 5542–5556.

[29] H. Mamtaz, M.H. Fouladi, M. Al-Atabi, S.N. Namasivayam, Acoustic absorption of natural fiber composites, J. Eng. (United Kingdom). 2016 (2016). https://doi.org/10.1155/2016/5836107.

[30] K.L.N. Raj, K.G. Ashok, Design and Fabrication of Vibration Damping Pad Using Luffa Cylindrica Fiber Reinforced Polymer Composite, Int. J. Multidiscip. Res. Mod. Educ. ISSN. II (2016) 2454–6119. www.rdmodernresearch.org.

[31] K. Labeeba, D. Ramya Devi, B. Vedha Hari, Comprehensive Review on Potential Applications of Natural Luffa Cylindrica Fibers, in: Phytopharm. Drug Deliv. Approaches, advidscience, 2019: pp. 02–17. https://doi.org/10.29290/pdda.1.7.2019.2-17.

[32] H. Demir, A. Top, D. Balköse, S. Ülkü, Dye adsorption behavior of Luffa cylindrica fibers, J. Hazard.

Mater. 153 (2008) 389–394. https://doi.org/10.1016/j.jhazmat.2007.08.070.

[33] M.A. Azeez, O.S. Bello, A.O. Adedeji, Traditional and Medicinal Uses of Luffa cylindrica: A Review, J. Med. Plants Stud. 1 (2013) 102–111.

[34] P.F. Souza Lima, A.L. Teixido, E.A. Sousa Paiva, Herbivory-induced overcompensation and resource-dependent production of extrafloral nectaries in Luffa cylindrica (Cucurbitaceae), Acta Oecologica. 93 (2018) 1–6. https://doi.org/10.1016/j.actao.2018.10.001.

[35] J.F. Jamaluddin, A. Firouzi, M.R. Islam, A.N.A. Yahaya, Effects of luffa and glass fibers in polyurethane-based ternary sandwich composites for building materials, SN Appl. Sci. 2 (2020) 1–10. https://doi.org/10.1007/s42452-020-3037-0.

[36] S.K. Saw, R. Purwar, S. Nandy, J. Ghose, G. Sarkhel, Fabrication, characterization, and evaluation of Luffa cylindrica fiber reinforced epoxy composites, BioResources. 8 (2013) 4805–4826. https://doi.org/10.15376/biores.8.4.4805-4826.

[37] K. Raja, B. Prabu, P. Ganeshan, V.S. Chandra Sekar, B. NagarajaGanesh, Characterization Studies of Natural Cellulosic Fibers Extracted from Shwetark Stem, J. Nat. Fibers. (2020) 1–12. https://doi.org/10.1080/15440478.2019.1710650.

[38] V.O.A. Tanobe, T.H.D. Sydenstricker, M. Munaro, S.C. Amico, A comprehensive characterization of chemically treated Brazilian sponge-gourds (Luffa cylindrica), Polym. Test. 24 (2005) 474–482. https://doi.org/doi:10.1016/j.polymertesting.2004.12.004.

[39] M. El-Roz, Z. Haidar, L. Lakiss, J. Toufaily, F. Thibault-Starzyk, Immobilization of TiO2 nanoparticles on natural Luffa cylindrica fibers for photocatalytic applications, RSC Adv. 3 (2013) 3438–3445. https://doi.org/10.1039/c2ra22438k.

[40] V. Valtchev, S. Mintova, Bioinspired Porous Materials, in: V. Valtchev, S. Mintova, M. Tsapatsis (Eds.), Ordered Porous Solids, Elsevier B.V., 2009: pp. 477–499. https://doi.org/10.1016/B978-0-444-53189-6.00018-4.

[41] J.P. Chen, T.C. Lin, Loofa sponge as a scaffold for culture of rat hepatocytes, Biotechnol. Prog. 21 (2005) 315–319. https://doi.org/10.1021/bp049684v.

[42] C. Liao, Y. Li, S.C. Tjong, Visible-light active titanium dioxide nanomaterials with bactericidal properties, Nanomaterials. 10 (2020). https://doi.org/10.3390/nano10010124.

[43] S. Zhang, X. Liang, G.M. Gadd, Q. Zhao, Advanced titanium dioxide-polytetrafluorethylene (TiO2-PTFE) nanocomposite coatings on stainless steel surfaces with antibacterial and anti-corrosion properties, Appl. Surf. Sci. 490 (2019) 231–241. https://doi.org/10.1016/j.apsusc.2019.06.070.

[44] S. Muduli, O. Game, V. Dhas, K. Vijayamohanan, K.A. Bogle, N. Valanoor, S.B. Ogale, TiO2-Au plasmonic nanocomposite for enhanced dye-sensitized solar cell (DSSC) performance, Sol. Energy. 86 (2012) 1428–1434. https://doi.org/10.1016/j.solener.2012.02.002.

[45] A. Pandikumar, R. Ramaraj, TiO2-Au nanocomposite materials modified photoanode with dual sensitizer for solid-state dye-sensitized solar cell, J. Renew. Sustain. Energy. 5 (2013) 1–10. https://doi.org/10.1063/1.4812641.

[46] S. Filice, G. Compagnini, R. Fiorenza, S. Scirè, L. D'Urso, M.E. Fragalà, P. Russo, E. Fazio, S. Scalese, Laser processing of TiO2 colloids for an enhanced photocatalytic water splitting activity, J. Colloid Interface Sci. 489 (2017) 131–137. https://doi.org/10.1016/j.jcis.2016.08.013.

[47] A. Gruger, A. Régis, T. Schmatko, P. Colomban, Nanostructure of Nafion® membranes at different

states of hydration: An IR and Raman study, Vib. Spectrosc. 26 (2001) 215–225. https://doi.org/10.1016/S0924-2031(01)00116-3.

[48] A. Kharoubi, A. Bouaza, B. Benrabah, A. Ammari, A. Khiali, Characterization of Ni-doped TiO2 thin films deposited by dip-coating technique, EPJ Appl. Phys. 72 (2015) 1–7. https://doi.org/10.1051/epjap/2015150282.

[49] P.A. Ubi, S. Abdul, R. Asipita, Effect of Sodium Hydroxide Treatment on the Mechanical Properties of Crushed and Uncrushed Luffa cylindrica Fibre Reinforced rLDPE Composites, Int. J. Mater. Metall. Eng. 9 (2015) 203–208.

[50] C. Chung, M. Lee, E.K. Choe, Characterization of cotton fabric scouring by FT-IR ATR spectroscopy, Carbohydr. Polym. 58 (2004) 417–420. https://doi.org/10.1016/j.carbpol.2004.08.005.

[51] M. Sahli, A. Cablé, K. Chetehouna, S. Hamamda, N. Gascoin, S. Revo, Preparation and characterization of polytetrafluoroethylene (PTFE)/Thermally Expanded Graphite (TEG) nanocomposites, Compos. Part B Eng. 124 (2017) 175–181. https://doi.org/10.1016/j.compositesb.2017.05.046.

[52] C.Y. Liang, S. Krimm, Infrared spectra of high polymers. III. Polytetrafluoroethylene and polychlorotrifluoroethylene, J. Chem. Phys. 25 (1956) 563–571. https://doi.org/10.1063/1.1742964.

[53] J. Mihály, S. Sterkel, H.M. Ortner, L. Kocsis, L. Hajba, É. Furdyga, J. Minka, FTIR and FT-Raman spectroscopic study on polymer based high pressure digestion vessels, Croat. Chem. Acta. 79 (2006) 497–501.

[54] Y. Qian, L. Chi, W. Zhou, Z. Yu, Z. Zhang, Z. Zhang, Z. Jiang, Fabrication of TiO2 -modified polytetrafluoroethylene ultrafiltration membranes via plasma-enhanced surface graft pretreatment, Appl. Surf. Sci. 360 (2016) 749–757. https://doi.org/10.1016/j.apsusc.2015.11.059.

[55] M.M. Mossoba, M.P. Yurawecz, R.E. McDonald, Rapid determination of the total trans content of neat hydrogenated oils by attenuated total reflection spectroscopy, JAOCS, J. Am. Oil Chem. Soc. 73 (1996) 1003–1009. https://doi.org/10.1007/BF02523408.

[56] T.A. Khalyavka, N.D. Shcherban, V. V. Shymanovska, E. V. Manuilov, V. V. Permyakov, S.N. Shcherbakov, Cerium-doped mesoporous BaTiO3/TiO2 nanocomposites: structural, optical and photocatalytic properties, Res. Chem. Intermed. 45 (2019) 4029–4042. https://doi.org/10.1007/s11164-019-03888-z.

[57] Y. Laidani, S. Hanini, G. Mortha, G. Heninia, Study of a fibrous annual plant, Luffa Cylindrica for ppaper application Part I: Characterization of the Vegetal, Iran. J. Chem. Chem. Eng. 31 (2012) 119–129.

[58] N. Grange, K. Chetehouna, N. Gascoin, S. Senave, Numerical investigation of the heat transfer in an aeronautical composite material under fire stress, Fire Saf. J. 80 (2016) 56–63. https://doi.org/10.1016/j.firesaf.2016.01.005.